

# Short-Range Correlation Induced Pseudogap in Doped Mott Insulators

B. Kyung, S. S. Kancharla, D. Sénéchal, A. -M. S. Tremblay  
*Département de physique and Regroupement québécois sur les matériaux de pointe,  
Université de Sherbrooke, Sherbrooke, Québec J1K 2R1, Canada*

M. Civelli, and G. Kotliar  
*Physics Department and Center for Materials Theory,  
Rutgers University, Piscataway, New Jersey 08855, USA*  
(Dated: February 8, 2020)

We study the evolution of a Mott-Hubbard insulator into a correlated metal upon doping in the two-dimensional Hubbard model using the Cellular Dynamical Mean Field Theory. Short-range spin correlations create two additional bands apart from the familiar Hubbard bands in the spectral function. Even a tiny doping into this insulator causes a jump of the Fermi energy to one of these additional bands and an immediate momentum dependent suppression of the spectral weight at this Fermi energy. This suggests a strong-coupling mechanism for the pseudogap phenomenon seen in several cuprates.

The issue of the origin of the pseudogap phenomenon observed in underdoped cuprates lies at the center of any theoretical explanation for high temperature superconductivity in the cuprates and is one of the most challenging questions in condensed matter physics. The suppression of low energy spectral weight in the normal state of these materials has been observed through various experimental probes [1]. In spite of many theoretical works to explain the observed anomalies, there is no consensus at present. The lack of controlled approximations to deal with the strong coupling physics and low dimensionality inherent to these systems continues to pose major stumbling blocks towards a complete theoretical understanding. Since the parent compounds of the cuprates are Mott-Hubbard insulators, an understanding of the evolution of such an insulator into a correlated metal upon doping is crucial.

In this paper we address the issue of the emergence of the pseudogap phenomenon on doping a Mott-Hubbard insulator with Cellular Dynamical Mean-Field Theory (CDMFT) [2]. The CDMFT method is a natural generalization of the single site DMFT [3] to incorporate short-range spatial correlations. This method [4] has already passed several stringent tests against exact results obtained by the Bethe Ansatz and the Density Matrix Renormalization Group (DMRG) techniques in one dimension, where the CDMFT scheme is expected to be in the worst case scenario. Long-range order involving several lattice sites such as  $d$ -wave superconductivity can be also described in CDMFT. Several other cluster schemes have been recently proposed [5]. The Dynamical Cluster Approximation (DCA) [6] is a cluster scheme in momentum space, wherein the cluster considered, if regarded in real space, has periodic boundary conditions. Another approach [7] uses a continuous interpolation of the self-energy in momentum space in the self-consistency condition. In Cluster Perturbation Theory (CPT) [8] the lattice self-energy is approximated by the self-energy of

the cluster only, whereas in its variational extension (V-CPT) [9], the cluster self-energy is determined by a rigorous variational principle for the one-body part of the cluster Hamiltonian. That principle allows one to consider CPT, V-CPT and CDMFT within a unified framework.

In the CDMFT construction [2, 4] the infinite lattice is tiled with identical clusters of size  $N_c$ . In an effective action description, the degrees of freedom in a single cluster are treated exactly, while the remaining ones are replaced by a bath of non-interacting electrons, which hybridize with the cluster degrees of freedom. For practical purposes, it is useful to view this cluster action as arising from a cluster-bath Hamiltonian of the form

$$H = \sum_{\langle\mu\nu\rangle,\sigma} t_{\mu\nu} c_{\mu\sigma}^\dagger c_{\nu\sigma} + U \sum_{\mu} n_{\mu\uparrow} n_{\mu\downarrow} + \sum_{m,\sigma} \varepsilon_{m\sigma} a_{m\sigma}^\dagger a_{m\sigma} + \sum_{m,\mu,\sigma} V_{m\mu\sigma} (a_{m\sigma}^\dagger c_{\mu\sigma} + \text{H.c.}) \quad (1)$$

Here the indices  $\mu, \nu = 1, \dots, N_c$  label sites within the cluster,  $m = 1, \dots, N_b$  with  $N_b$  representing the number of bath degrees of freedom, and  $c_{\mu\sigma}$  and  $a_{m\sigma}$  annihilate electrons on the cluster and the bath, respectively.  $t_{\mu\nu}$  is the hopping matrix within the cluster,  $\varepsilon_{m\sigma}$  is the bath energy and  $V_{m\mu\sigma}$  is the bath-cluster hybridization matrix. Let us adopt a matrix notation (cluster indices suppressed) for the hopping matrix  $t$ , the cluster Green function  $G_c(i\omega)$ , its noninteracting counterpart  $G_0(i\omega)$  and the cluster self-energy  $\Sigma = G_0^{-1} - G_c^{-1}$ . We start with an initial guess for the bath parameters  $\varepsilon_{m\sigma}$  and  $V_{m\mu\sigma}$  (respecting four-fold symmetry of the cluster) which determines a starting  $G_0(i\omega)$ . With this guess the cluster Green function is calculated by solving the cluster-bath Hamiltonian (Eq. 1). To close the self-consistency loop

we obtain a new  $G_0(i\omega)$  using

$$G_0^{-1}(i\omega_n) = \left( \frac{N_c}{(2\pi)^2} \int d\vec{K} \frac{1}{i\omega_n + \mu - t(\vec{K}) - \Sigma(i\omega_n)} \right)^{-1} + \Sigma(i\omega_n). \quad (2)$$

Here  $t$  depends on  $\vec{K}$ , the wave vector of the superlattice Brillouin zone, because of inter-cluster hopping. Now to invert the relation between this  $G_0(i\omega)$  and the bath parameters for the next iteration we minimize

$$d = \sum_{\omega_n, \mu, \nu} \left| \left( G_0^{-1}(i\omega_n) - G_{0, \text{proj}}^{-1}(i\omega_n) \right)_{\mu\nu} \right|^2, \quad (3)$$

where  $G_{0, \text{proj}}^{-1}(i\omega_n)$  denotes the Weiss field projected onto a finite bath. The lattice Green function  $G(\vec{k}, i\omega_n)$  is obtained in terms of the cluster self-energy

$$G(\vec{k}, i\omega_n) = \frac{1}{N_c} \sum_{\mu\nu} e^{i\vec{k} \cdot (\vec{r}_\mu - \vec{r}_\nu)} \left[ \frac{1}{i\omega_n + \mu - t(\vec{K}) - \Sigma(i\omega_n)} \right]_{\mu\nu}$$

All quantities plotted in this paper are derived from this lattice Green function. This is different from the periodization of the self-energy in Ref. [4, 10].

In the present study we used  $N_c = 4$  sites for the cluster (minimum number of sites reflecting the full square lattice symmetry) and  $N_b = 8$  sites for the bath, and solved the cluster-bath Hamiltonian (Eq. 1) by the exact diagonalization method [11] at zero temperature. The self-consistency condition (Eq. 2) was imposed on the imaginary frequency axis (with a cutoff of  $1.5t$ ), since

$G_0(i\omega_n)$  is a smooth function without any poles. Most dynamical quantities were computed directly in real frequency with a Lorentzian width of  $0.1t$ . All of the results were obtained for the particle-hole symmetric model with just nearest neighbor hopping.

In order to see how the Mott transition occurs due to short-range correlations and how the differences between short- and long-range correlation effects evolve with interaction strength, we present in Fig. 1 the density of states  $N(\omega)$  as computed from the paramagnetic (P) (solid curves) and the antiferromagnetic (AF) (dashed curves) states at half-filling ( $n = 1$ ). The two states (P and AF) are selected by imposing appropriate constraints on the bath parameters. When the correlation length is larger than the size of a cluster, long-range effects are expected to be well described by the solution with the corresponding long-range order. The difference between the two solutions at low energies is largest at weak coupling ( $U = 4t, 5t$ ) and decreases at strong coupling ( $U \gtrsim 8t$ ). In the weak coupling case,  $N(\omega)$  has only a small dip at the Fermi energy compared to the AF solution, indicating that short-range correlations available in a cluster of size  $N_c = 4$  are not long enough to lead to an insulating gap [12, 13]. As  $U$  is increased to  $6t$ , two sharp bands begin to develop at the gap edge and become well separated from the Hubbard bands centered around  $\pm U/2$ . At this strength of  $U$ , the two solutions (P and AF) start approaching each other at low energies. When  $U = 8t$ , long-range correlations (dashed curve) sharpen the low energy bands but they stay essentially at the same energy. Thus short-range correlations begin to dominate the Physics. At this value of  $U$  the low energy inner bands are clearly distinguishable from the Hubbard bands coming from local correlations and the insulating gap is clearly defined. Since these bands are missed in the single site DMFT [14] and smoothly evolve into sharp spin density wave-like bands when AF order is allowed, they are attributed to *short-range spin* correlations. This is further evidenced by their dispersions of about  $2J \sim 2\frac{4t^2}{U} = t$ . When  $U$  is further increased beyond the bandwidth of  $8t$  (not shown), the distance between the low energy bands increases, but the relative shape and position of the inner and the Hubbard bands are unchanged.

Next we investigate the evolution of a Mott-Hubbard insulator into a correlated metal upon a small electron doping at  $U = 8t$ . It is clear at half-filling (Fig. 2(a)) that  $A(\vec{k}, \omega)$  (and also  $N(\omega)$  in Fig. 1) shows four significant features near  $(0, \pi)$  and  $(\pi/2, \pi/2)$ . The four peak (or band) structure in  $A(\vec{k}, \omega)$  was previously found by Moreo *et al.* [15] and Preuss *et al.* [16] in their high resolution Quantum Monte Carlo (QMC) results for the half-filled 2D Hubbard model. The most striking feature of even a tiny doping into a Mott-Hubbard insulator (Fig. 2(b) and (c)) is that one of the inner bands at

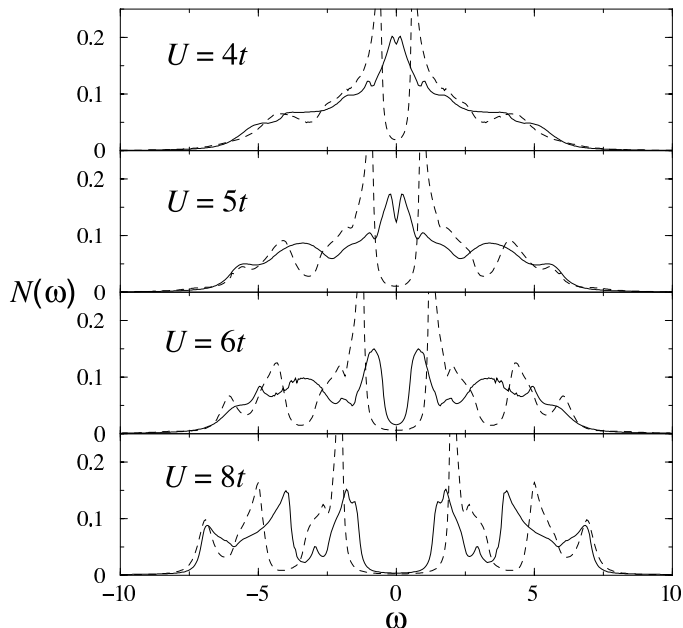


FIG. 1: Density of states  $N(\omega)$  at half-filling ( $n = 1$ ) for several values of  $U$ . The dashed curves are  $N(\omega)$  with AF long-range order.

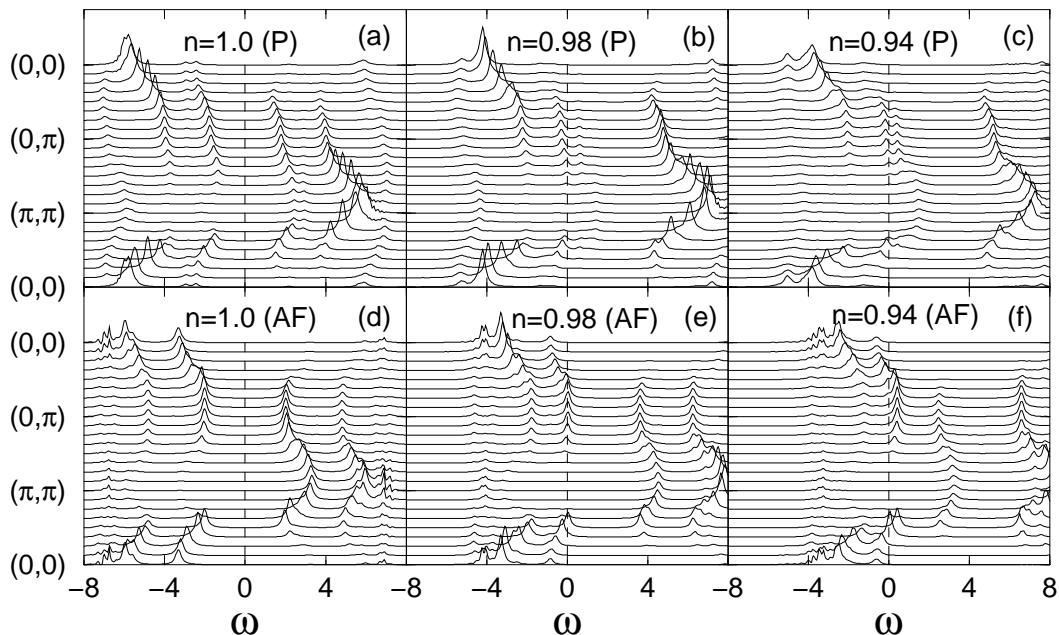


FIG. 2: Spectral function  $A(\vec{k}, \omega)$  along some symmetry directions in the paramagnetic normal (upper row) and the AF (lower row) states for several small dopings with  $U = 8t$ . The dashed lines represent the Fermi energy.

$\omega > 0$  disappears almost immediately, while the Fermi energy jumps to the other band that persists at  $\omega < 0$ . Furthermore, one already sees here the pseudogap phenomenon. Peaks crossing the Fermi level exist near  $(\pi/2, \pi/2)$ , while near  $(0, \pi)$  the spectral weight is minimum at the Fermi energy, instead of maximum. That minimum occurs between the two peaks as can be seen more clearly at the largest doping in Fig. 2. As we will see shortly, the suppression of weight near the Fermi energy persists up to about 20% doping. These features (Fig. 1 and Fig. 2(a)(b)(c)) offer a systematic picture of how the pseudogap phenomenon arises upon doping a Mott-Hubbard insulator. The appearance of a low energy peak together with one at high binding energy is consistent with exact diagonalization results for the  $t - J$  model [15, 17]. We also show clear differences between the momentum resolved spectra of the paramagnetic and the AF states. The main differences for the AF case at half-filling, Fig. 2(d), are that the low-energy bands are more intense than in the paramagnetic state Fig. 2(a) and that they bend back near  $(0, \pi)$  and near  $(\pi/2, \pi/2)$ , reflecting the underlying AF symmetry. The results of Fig. 2(d) are strikingly similar to those obtained in a 10 site V-CPT calculation [18]. The more drastic differences between the paramagnetic and AF solutions occur at finite doping. While in both cases the Fermi level immediately jumps to the closest low energy band upon doping, Figs. 2(e) and (f) [19] show that, in the AF solution, the four peak structure is preserved and the excitations at the Fermi energy are quite sharp.

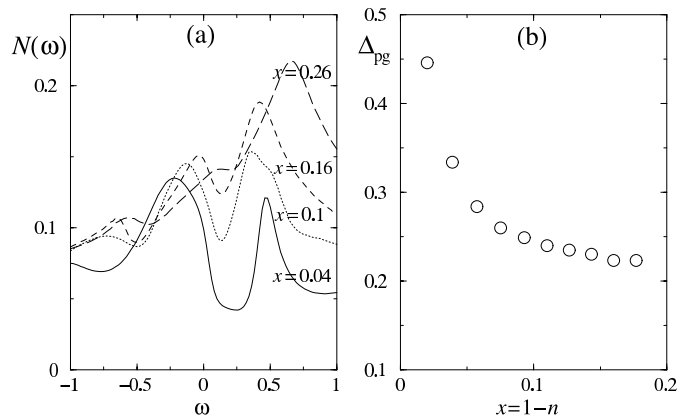


FIG. 3: (a) Density of states  $N(\omega)$  for several doping levels with  $U = 8t$ . The solid, dotted, dashed, and long-dashed curves correspond to  $x = 0.04, 0.1, 0.16,$  and  $0.26$ , respectively. (b) Pseudogap size determined as the half-distance between the two peaks in  $N(\omega)$  for  $U = 8t$ .

Fig. 3(a) shows the density of states  $N(\omega)$  for several dopings. The pseudogap found here occurs over a scale  $0.4t - 0.5t$  and is more clearly resolved in comparison with previous works [6, 20]. Furthermore, the pseudogap size increases with decreasing doping (Fig. 3(b)), consistent with recent experiments in the cuprates [1, 21]. The pseudogap feature vanishes for large enough doping not because the two peaks coalesce but because of a gradual filling up of the spectral weight between the two peaks. The appearance of a pseudogap near  $x = 0.2$  found in the single particle spectrum coincides with the downturn of

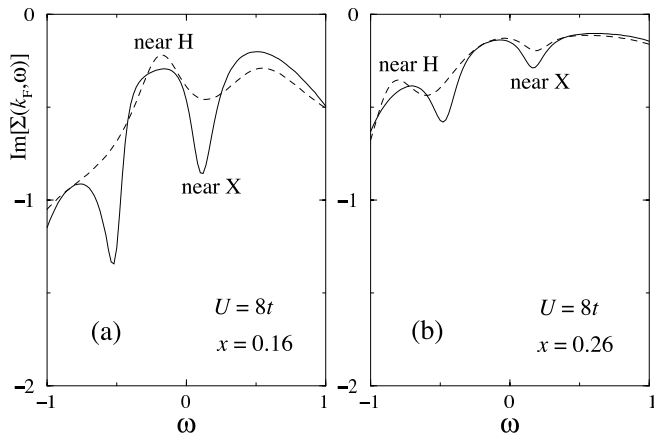


FIG. 4: Imaginary part of the self-energy at Fermi wave vectors for (a)  $x = 0.16$  and (b)  $x = 0.26$  with  $U = 8t$ .  $X = (0, \pi)$  and  $H = (\pi/2, \pi/2)$ .

the uniform cluster spin susceptibility (not shown), suggesting that the pseudogap has to do with spin singlet formation of correlated electrons.

The significant differences of spectral properties at  $x = 0.16$  and  $x = 0.26$  (Fig. 3 (a)) can be understood in terms of self-energies [22]. Fig. 4(a) shows the imaginary part of the self-energy for  $x = 0.16$  at the Fermi wave vectors near  $(0, \pi)$  and  $(\pi/2, \pi/2)$ . The scattering rate becomes large near X in particular, leading to the pseudogap in both  $N(\omega)$  and  $A(\vec{k}, \omega)$  (not shown here). However, Fig. 4(b) shows much smaller self-energy in magnitude for  $x = 0.26$ , leading toward the Fermi liquid at large doping. Clearly, upon doping a Mott insulator into a metallic state, quasiparticles disappear since the absolute value of the imaginary part of the self-energy is a local maximum at the Fermi energy instead of minimum as in a Fermi liquid picture (see caveat [23]). The large scattering rate leading to the pseudogap found here is reminiscent of that due to the presence of the large density of states for scattering at the van Hove singularity in the weak coupling case. With a finite second-neighbor hopping  $t'$ , the crossing of the non-interacting Fermi surface and the AF Brillouin zone boundary would lead to additional scattering processes [22].

It is remarkable that including only the nearest neighbor correlations into this two-dimensional model is able to capture the details of the spectral properties which are missed in the single site DMFT. We stress that at *weak* coupling and in two dimensions, a different mechanism involving large AF correlation lengths causes the pseudogap [12, 22, 24, 25]. That mechanism, relevant for electron-doped cuprates near optimal doping, is clearly not involved in the present *strong* coupling case because we saw that in the doped AF state there is no gap or pseudogap at the Fermi energy while in the paramagnetic normal state an AF correlation length limited to the cluster size suffices to create the pseudogap. Although the sizes of clusters accessible to computation limit the resolution

of the spectral properties, we expect the above picture for the *strong* coupling pseudogap to be robust with respect to an increase in the cluster size. As previously observed in CPT [22] and in another CDMFT calculation [10] we found that including realistic band structure parameters such as second- and third-neighbor hoppings can explain the observed asymmetry in the apparent Fermi surface of hole- and electron-doped cuprates. A strong shape renormalization was also quantified in Ref. [10].

In conclusion, the long standing problem of the evolution of a Mott-Hubbard insulator into a correlated metal upon doping has been examined in the two dimensional Hubbard model by using the Cellular Dynamical Mean Field Theory (CDMFT) which incorporates short-range spatial correlations. At half-filling these correlations create two additional bands besides the familiar Hubbard ones. Even a tiny doping into a Mott-Hubbard insulator causes the Fermi energy to jump to one of these bands and the spectral weight to be suppressed immediately in a  $\vec{k}$  dependent way, such that a pseudogap appears near  $(\pi, 0)$  while a peak survives near  $(\pi/2, \pi/2)$ . When AF long-range order is present at finite doping, the picture is quite different, demonstrating that at strong coupling the pseudogap in the particle-hole symmetric model is a short-range effect. This provides a systematic physical picture for the emergence of the strong coupling pseudogap phenomenon in doped Mott-Hubbard insulators and the consequent non-Fermi liquid behavior that arises solely from short-range spin correlations and large scattering rates, without any symmetry breaking.

We thank O. Parcollet for useful discussions. The present work was supported by NSERC (Canada), FQRNT (Québec), CFI (Canada), CIAR, the Tier I Canada Research Chair Program (A.-M.S.T.), and the NSF under grant DMR-0096462 (G.K.).

- 
- [1] T. Timusk *et al.*, Rep. Prog. Phys. **62**, 61 (1999).
  - [2] G. Kotliar *et al.*, Phys. Rev. Lett. **87**, 186401 (2001).
  - [3] A. Georges *et al.*, Rev. Mod. Phys. **68**, 13 (1996).
  - [4] G. Biroli *et al.*, Phys. Rev. B **65**, 155112 (2002); C. Bolech *et al.*, Phys. Rev. B **67**, 075110 (2003); M. Capone *et al.*, Phys. Rev. B **69**, 195105(2004).
  - [5] T. Maier *et al.*, cond-mat/0404055.
  - [6] M. H. Hettler *et al.*, Phys. Rev. B **58**, R7475 (1998); M. Jarrell *et al.*, Europhys. Lett. **56**, 563 (2001); T. Maier *et al.*, Phys. Rev. Lett. **92**, 027005 (2004).
  - [7] A. I. Lichtenstein *et al.*, Phys. Rev. B **62**, R9283 (2000).
  - [8] D. Sénéchal *et al.*, Phys. Rev. Lett. **84**, 522 (2000).
  - [9] M. Potthoff, Eur. Phys. J. B **32**, 429 (2003).
  - [10] M. Civelli *et al.*, cond-mat/0411696.
  - [11] M. Caffarel *et al.*, Phys. Rev. Lett. **72**, 1545 (1994).
  - [12] B. Kyung *et al.*, Phys. Rev. Lett. **90**, 099702 (2003).
  - [13] S. Moukouri *et al.*, Phys. Rev. Lett. **87**, 167010 (2001).
  - [14] At half-filling the gross features found in the CDMFT may be qualitatively described by the AF solution of the

- single site DMFT (M. Rozenberg *et al.*, Phys. Rev. B **54**, 8452 (1996)).
- [15] A. Moreo *et al.*, Phys. Rev. B **51**, 12045 (1995).
  - [16] R. Preuss *et al.*, Phys. Rev. Lett. **75**, 1344 (1995).
  - [17] E. Dagotto, Rev. Mod. Phys. **66**, 763 (1994).
  - [18] C. Dahnken *et al.*, Phys. Rev. B **70**, 245110 (2004).
  - [19] For  $U = 8t$  and  $t' = 0$  the AF solution disappears for  $x = 1 - n \geq 0.08$ .
  - [20] T. Stanescu *et al.*, Phys. Rev. Lett. **91**, 017002 (2003).
  - [21] A. Damascelli *et al.*, Rev. Mod. Phys. **75**, 473 (2003).
  - [22] D. Sénéchal *et al.*, Phys. Rev. Lett. **92**, 126401 (2004).
  - [23] Due to the finite bath and cluster sizes, our calculations are limited to an energy resolution of about  $0.1t$ . Hence the possibility of a Fermi liquid regime at lower energies cannot be ruled out.
  - [24] B. Kyung *et al.*, Phys. Rev. Lett. **93**, 147004 (2004).
  - [25] V. Hankevych *et al.*, cond-mat/0407085